Granular response to impact: Topology of the force networks

T. Takahashi,[1] Abram H. Clark,[2] T. Majmudar,[3] and L. Kondic[1]
[1]*Department of Mathematical Sciences, New Jersey Institute of Technology, Newark, New Jersey 07102, USA*
[2]*Department of Physics, Naval Postgraduate School, Monterey, California 93943, USA*
[3]*Department of Mathematics, New York University, New York, New York 10012, USA*

(Received 20 September 2017; published 12 January 2018)

The impact of an intruder on granular matter leads to the formation of mesoscopic force networks, which were seen particularly clearly in the recent experiments carried out with photoelastic particles [Clark *et al.*, Phys. Rev. Lett. **114**, 144502 (2015)]. These force networks are characterized by complex structure and evolve on fast time scales. While it is known that total photoelastic activity in the granular system is correlated with the acceleration of the intruder, it is not known how the structure of the force network evolves during impact, and if there are dominant features in the networks that can be used to describe the intruder's dynamics. Here, we use topological tools, in particular persistent homology, to describe these features. Persistent homology allows quantification of both structure and time evolution of the resulting force networks. We find that there is a clear correlation of the intruder's dynamics and some of the topological measures implemented. This finding allows us to discuss which properties of the force networks are most important when attempting to describe the intruder's dynamics. In particular, we find that the presence of loops in the force network, quantified by persistent homology, is strongly correlated to the deceleration of the intruder. In some cases, particularly for the impact on soft particles, the measures derived from the persistence analysis describe the deceleration of the intruder even better than the total photoelastic activity. We are also able to define an upper bound on the relevant time scale over which the force networks evolve.

DOI: 10.1103/PhysRevE.97.012906

I. INTRODUCTION

When a high-speed intruder strikes a granular material, its momentum is carried away and dissipated by the grains. This process is important in a wide variety of natural and man-made settings, including astrophysics [1,2], rugged-terrain robotics [3,4], and ballistics [5]. Previous experimental studies [6–20] have developed macroscopic descriptions involving, for example, the dynamics of the intruder [7,13,14], the size of the impact crater [10,12], collective dynamics of multiple intruders [15], the influence of bed preparation [16], or the influence of interstitial fluid [18,20]. However, relating macroscopic behavior to physical processes at the grain scale or at intermediate length scales can be quite difficult, primarily because measuring forces and dynamics inside the granular material is not possible in most experimental realizations.

Recent experiments on granular impact using photoelastic disks [21–24] and high-speed video (frame rates of 10–50 kHz) have provided some insight into the complex nature of grain-grain force transmission within the granular material during initial impact [25] and penetration [26]. This allows visualization of the force networks that form during impact, and these forces can then be connected to the intruder dynamics [26–28] or the motion of grains [29]. However, a complete description of the relationship between the intruder motion and the space- and time-dependent granular forces is still lacking, partially because the images from high-speed videos lack the spatial resolution required to quantitatively measure vector forces [30,31] between grains. Quantitative photoelastic measurements are thus limited to, for example, the total photoelastic intensity in a certain region of the image, which gives an estimate of the pressure in that region.

In recent years, significant progress has been made toward an understanding of force networks using tools such as statistical methods [32–34], network analysis [35–37], and application of topological methods [38–43]. A significant part of the research involving consideration of topology of force networks has been carried out based on persistence homology; see [42] for in-depth discussion of the application of this technique to granular matter, and [43] for a brief overview. In this context, persistent homology is based on reducing the complex information contained in force networks to point clouds, called persistence diagrams, that describe the underlying networks. Persistence diagrams are computed by varying the force threshold and measuring the threshold value at which various components of the network appear and disappear. Commonly, this filtering is carried out by considering superlevel sets, where the topological measures are computed on the force values above the threshold. As the force threshold is continuously decreased from the maximum value to the minimum value, individual components appear (they are "born"), connect (during this process, one of the components "dies"), and/or form loops.

While this outlined reduction leads to some loss of information, the persistence diagrams have been very useful in describing the force networks for compressed granular systems [40,41,43], as well as in helping to identify the influence of particle shape on the properties of force networks [44,45]. It should be pointed out, however, that until now the tools of persistence homology, as well as the other techniques listed

above, have been applied mostly to the data resulting from simulations, and there have been no attempts so far to analyze the properties of force networks that emerge during dynamic experimental processes evolving on fast time scales.

In this work, we apply the techniques of persistent homology to analyze the granular force networks that form during impacts into photoelastic disks. In the present context, persistent homology involves a topological characterization of a scalar field, in this case the brightness of a given photoelastic image from a high-speed movie of a granular impact event. The resulting topological measures can give detailed information about the granular response at a spatial scale that is larger than a grain but small compared to the size of the granular assembly. By analyzing a time series of photoelastic images, we show that persistence homology can be used to tie the granular force response to the intruder dynamics, In many cases, persistence homology provides a more detailed connection than simply measuring the total photoelastic intensity. In addition, our topological analysis suggests that the presence of loops in the force network plays a crucial role in decelerating the intruder. In this work, we attempt to use topology-based methods to analyze the results of physical experiments on granular materials involving fast dynamics.

The rest of this paper is organized as follows. In Sec. II we discuss the techniques used to analyze the results, including experimental techniques, image processing, and a brief description of the used topology-based measures. In Sec. III we discuss the main results, including both structural and time-dependent properties of the force networks. Section IV gives conclusions and outlook.

II. TECHNIQUES

A. Experimental techniques

We perform a topological analysis on images from high-speed impacts into a collection of photoelastic disks (3 mm thick), which are confined between two Plexiglas sheets (0.91 m $\times$ 1.22 m $\times$ 1.25 cm) separated by a thin gap (3.3 mm). The experimental apparatus is identical to that used in previous experiments [25–28]. Circular intruders are machined from a bronze sheet (with a bulk density of 8.91 g/cm^3 and a thickness of 0.23 cm) of diameters D of 6.35, 12.7, and 20.32 cm. We drop these intruders from varying heights through a shaft connected to the top of the apparatus, yielding an impact velocity $v_0 \leqslant 6.6$ m/s. We record the results with a Photron FASTCAM SA5 at frame rates of up to 25 000 frames per second (fps). To measure v_0, we track the intruder and take a numerical derivative as in [25–28].

Photoelastic particles are cut from a polyurethane sheet from Precision Urethane into disks. Granular samples are all bidisperse, containing a mixture of disks with diameters of 6 and 9 mm in roughly equal numbers. We use two different sets of particles with distinct stiffnesses: Shore 60A (with a bulk elastic modulus of roughly 1–10 MPa) and Shore 80A (with a bulk elastic modulus of roughly 10–100 MPa). We give a more comprehensive treatment of the physical properties of these particles, including a relation of force as a function of compression, in Ref. [25]. Following [25], we refer to Shore 60A particles as soft and Shore 80A particles as medium stiffness.

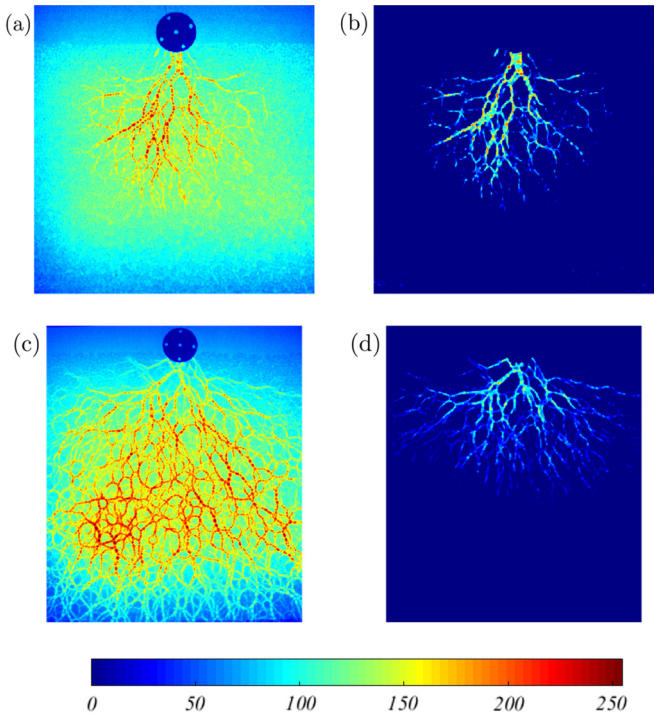

FIG. 1. Example of image processing for (a), (b) medium (6.35–4.5) and (c), (d) soft (6.35–1.3) particles. Here, (a), (c) are raw images, and (b), (d) show the postprocessed images (using the MATLAB jet color scheme). See the text for details on image processing. Note in particular that our image-processing approach removes the preexisting force chains that are clearly visible at the bottom part in (c) but not in (d). The naming convention is such that the first number specifies the radius of the intruder in cm, and the second one specifies the impact speed in m/s. The images are shown at the times 0.276 ms (medium) and 16 ms (soft) after impact. We will refer to the medium 6.35–4.5 experiment as the *reference* one for the remainder of the paper.

B. Image processing

Figure 1 shows two examples of experimental images, for impact on medium (a), (b) and soft (c), (d) particles. We first remove noise from the initial images, (a), (c) in Fig. 1, by spatial homogenization to account for the inconsistent lighting as well as by applying a notch filter to remove the flickering of the ac light source at 120 Hz. We then perform image subtraction between each frame and a reference frame. The result is an 8-bit grayscale image that shows negligible temporal fluctuations or spatial inconsistencies in the lighting. We note that, for the soft particles, preexisting force chains from gravity are visible before impact, as seen in Fig. 1(c), and these are subtracted from the final images. After noise removal, we use built-in MATLAB functions to slightly dilate and erode the images to make sure gaps between neighboring grains in a force chain are connected. The final images are as shown in Figs. 1(b) and 1(d). The image processing we show is performed on the entire image.

Figures 1(a) and 1(b) correspond to medium stiffness particles, for which the speed of sound is roughly 90 m/s [25]. These images are recorded at 25 000 fps. For soft particles shown in Figs. 1(c) and 1(d), the estimated speed of sound is 30 m/s [25], and the frame rate here is 10 000 fps. The speed of sound divided by the frame rate gives the typical distance

of information propagation between two consecutive images of roughly 3 mm, which is about half of the smallest grain diameter. Thus, we record images sufficiently fast to resolve grain-grain force transmission during impact, although our results below suggest the possibility of evolution on even faster time scales.

C. Topological measures

In the context of granular matter, persistence homology computations have so far been reported for the data from numerical simulations. The results presented here constitute an attempt to extract useful information using persistent homology from experimental data. In our case, the data available, consisting of the images shown in the previous section, are by necessity incomplete, since the impact is a fast process involving a large number of particles. The spatial resolution of these images is not sufficient to resolve the photoelastic response at each grain-grain contact, therefore detailed information about the interparticle forces is not available. Thus, the question we address is whether useful information can be extracted from such data using persistent homology computations. If so, then the tools we discuss here could be applied to a broad range of experimental granular systems involving fast dynamics.

The details regarding applications of persistent homology to an analysis of force networks in granular matter could be found in previous works [42,43], and here we provide a brief overview. Before going into the description, it is important to point out one significant difference between the approach taken by persistence homology compared to more classical approaches, which typically consider the interparticle forces as a function of (often arbitrarily chosen) force threshold. Instead of using a threshold, persistent homology is able to treat the information about the forces on all levels at once. Therefore, separation into weak and strong force networks, for example, is not necessary, although it can be carried out if so desired. For the data considered in this paper, we will not even be considering forces on the level of contacts, as discussed above, but only on the level of image brightness.

Each experimental image could be considered as a rectangular array of pixels, with each pixel specified by its brightness value in the range $\theta \in [0:255]$. For each image, we carry out superlevel filtration, meaning that we consider the pixels with the brightness *above* a specified threshold as white, with the rest being black. Clearly, if we choose a very high threshold, only a few pixels will be white. Then, as we lower the threshold level, more and more pixels will become white. In simple terms, persistent homology keeps track of and quantifies the *connectivity* of the network that is formed by the white pixels. For a detailed discussion dealing with pixelized data in the context of particulate systems, we refer the reader to [42]; a less technical description can be found in [43]. We note, however, that the listed references focus on extracting force networks, since the data (either experimental examples or simulation results) included sufficient information to be able to extract the forces at each particle contact. This is not the case here, so we focus on the direct analysis of the pixelized images without attempting to formulate well-defined force networks. The codes used for computation of persistence are available online [46].

By the filtering process described above, each image can be associated with a corresponding persistence diagram (PD) that quantifies changes of the image as the filtering threshold, θ, is modified. There are two PDs for each image: PD_0 and PD_1, corresponding to the components and the loops, respectively. These diagrams encode the appearance and disappearance of connected components and loops by keeping track of the values of θ at which a component and/or loop appears or disappears. To facilitate interpretation, one could think of the connected components as "force chains" (for large values of θ). However, the idea of connected components is more general and more precisely defined than the somewhat vague "force chain" concept. PD_1 keeps track of the appearance and disappearance of loops, defined by the requirement that all pixels that form a loop are brighter than a specified value of θ. Connected components disappear when they merge (at some lower value of θ); the loops disappear when they get filled up with the pixels that are at least as bright as the specified threshold.

Figure 2 shows an example of PDs for one image from the reference experiment. On the horizontal axis we plot the birth (appearance) of a component or loop, and at the vertical axis we show the disappearance (death) coordinate. Part (a) shows the diagram for the components, PD_0, and part (b) shows the diagram for the loops, PD_1. Since components or loops are born before they die (that is, they appear on higher intensity levels than the ones on which they disappear), all the points (generators) are below the diagonal. To guide the reader in interpreting these diagrams, we provide a few brief remarks:

(i) Note the large number of generators close to the diagonal. These are generators that persist just for a small range of brightness values and could be considered as noise.

(ii) The dominant features (such as strong "force chains") are described by the generators that are farther away from the diagonal, and which are born at high values of θ.

(iii) Note that the birth values of PD_1 are lower than those of PD_0. This is due to the fact that the birth of a loop corresponds to the lowest magnitude of the pixels that form the loop.

These PDs are essentially point clouds that describe (in a simplified manner) complex network structure. They are still, however, rather complex since they include information about the connectivity of the networks over *all* brightness levels. Therefore, one must have an approach for their analysis and quantification. While there are different quantities that could be used for this purpose, in the present context we find it useful to consider the following simple measures:

(i) *Lifespan:* Consider a generator that got born on the level $\theta = b$ and died on the level $\theta = d$. The lifespan is then defined as b–d. The lifespans for the PDs shown in Figs. 2(a) and 2(b) are given in parts (c) and (d), respectively, of the same figure. We note that small lifespans occur very often, saying that there are many generators very close to the diagonals. In our data analysis presented in the next section, we find it convenient in some cases to remove such small lifespans from consideration, since the corresponding generators could be thought of as a consequence of noise in the experimental images.

(ii) *Total persistence* (TP) is defined as the sum of all lifespans, $\mathrm{TP(PD)} = \sum_{(b,d)\in \mathrm{PD}} (b\text{–}d)$. TP allows us to describe a whole PD by a single number at the cost of a significant information loss. If we think of the original image as a landscape (with the altitude corresponding to pixel brightness),

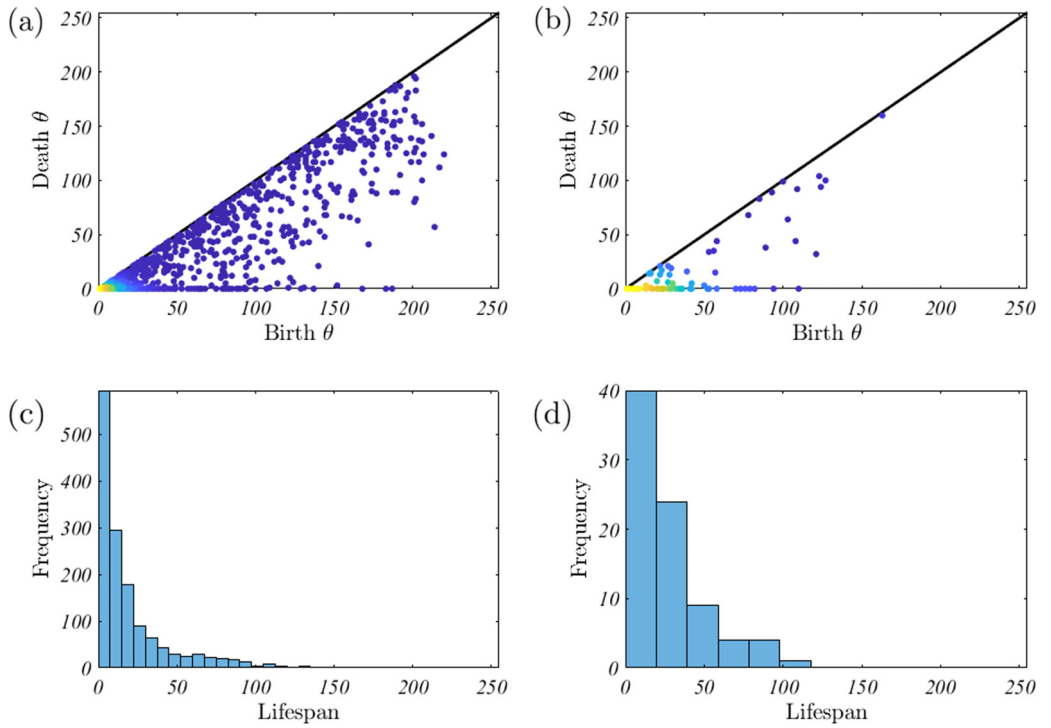

FIG. 2. Persistence diagrams (PDs) for the reference experiment (medium 6.25–4.5) (same time as shown in Fig. 1). Parts (a) and (b) show the PDs for components and loops, PD_0 and PD_1, respectively. Parts (c) and (d) show the corresponding lifespans. The x-axis range corresponds to brightness, covering the full range [0 : 255]. Note the large number of generators with very small lifespans, showing that there are many points in the diagrams that are near the diagonals and represent essentially noise. The Supplemental Material [47] shows the PDs and lifespans for all considered images of the reference experiment.

then the TP essentially tells us how flat this landscape is: larger TP corresponds to the landscape that is more mountainlike, with lots of hills and valleys, while small TP corresponds to the landscape without too many features. Since we have PD_0 and PD_1, we define total persistence for the components and the loops, TP_0 and TP_1, respectively. Another related measure is the total number of generators, TC, again for the components, TC_0, and loops, TC_1.

(iii) *Betti numbers:* Betti numbers simply count the number of features, components, β_0, or loops, β_1, at a specified threshold level, θ. These quantities could be obtained by simple counting; persistence homology is not required for their definition or computation. However, they could also be obtained from the PDs by essentially summing the number of generators such that their birth coordinate is larger, and their death coordinate smaller, than a considered threshold, θ. It should be noted that Betti numbers are a function of θ, and therefore they contain much less information than PDs themselves.

Although it can be proven that PDs are stable with respect to noise (small changes of input data produce small changes in corresponding PDs), the same cannot be shown for Betti numbers [42]. This property of PDs and Betti numbers should be remembered in particular when dealing with potentially noisy data, as in this paper.

The final quantity that we discuss in this overview of topological measures is the concept of distance between the PDs obtained at two different times. Such a quantity is possible since the space in which PDs live is a metric space and therefore a distance can be defined. In particular, the distance concept that we define below is such that the distance is small if the PDs are similar; see [42,43] for more in-depth discussion. The metrics that we consider and define here is based on the entire diagram, i.e., we compare two diagrams by comparing all points in each diagram. Note that this comparison does not involve thresholding: this measure compares the images on all brightness levels.

Consider two persistence points $p_0 = (b_0,d_0)$ and $p_1 = (b_1,d_1)$. The distance between p_0 and p_1 is defined by $\|(b_0,d_0) - (b_1,d_1)\|_\infty := \max\{|b_0 - b_1|,|d_0 - d_1|\}$. Now, given two persistence diagrams PD and PD', let $\gamma : \mathsf{PD} \to \mathsf{PD}'$ be a bijection between points in the two persistence diagrams where we are allowed to match points of one diagram with points on the diagonal of the other diagram. The *degree-q Wasserstein distance*, $d_{W2}(\mathsf{PD},\mathsf{PD}')$, is obtained by considering for each bijection, γ, the quantity

$$\left(\sum_{p\in\mathsf{PD}} \|p - \gamma(p)\|_\infty^q\right)^{1/q}$$

and defining the distance between PD and PD' to be the minimum value of this quantity over all possible bijections. Stated formally,

$$d_{Wq}(\mathsf{PD},\mathsf{PD}') = \inf_{\gamma:\mathsf{PD}\to\mathsf{PD}'} \left(\sum_{p\in\mathsf{PD}} \|p - \gamma(p)\|_\infty^q\right)^{1/q}.$$

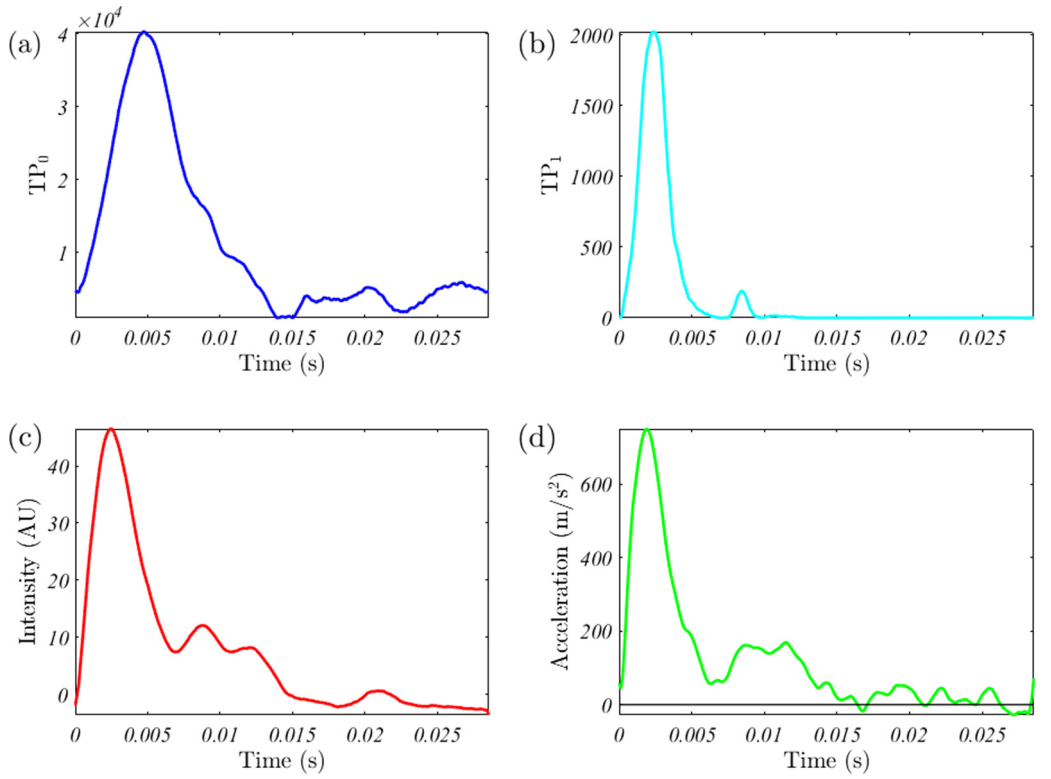

FIG. 3. Total persistence for the components, TP_0, for the loops, TP_1, the photoelastic intensity, and the intruder's acceleration for the reference case (medium 6.35–4.9). The Supplemental Material [47] shows the above curves jointly with the (processed) photoelastic images.

In simple terms, ones looks into the cheapest way to move the points of one diagram to those corresponding to the other diagram, remembering that the points could be moved to the diagonal as well. The cost of "moving the points" (i.e., selecting a given bijection) varies for different values of q. For example, the Wasserstein distance d_{W1} sums up all the differences with equal weight. For $q > 1$, the distance still keeps track of all the changes, but the small differences contribute less. For brevity, in this paper we use $q = 2$ only, and for simplicity of notation we use $d_{W2}(\beta_0)$ and $d_{W2}(\beta_1)$ to denote the distances between the components and for the loops, respectively. The code used for calculating distances is available online [46].

III. RESULTS

A. Material response: Structure and geometry

Figure 3 shows the results for the reference case. The four panels in the figure show the total persistence: TP_0, TP_1, the total photoelastic intensity, and the intruder's acceleration. Since the position data from which the intruder acceleration is computed are rather noisy, as discussed in [26], the velocity and acceleration are computed by numerical derivatives calculated based on a linear best fit to the data over a range of roughly 50 frames. This is equivalent to taking numerical derivatives and then smoothing with a low-pass filter. For consistency, the intensity and TP data, which are computed from photoelastic images, are also filtered using a similar procedure. However, the photoelastic signals here, using medium and soft particles, are not strongly fluctuating in time and thus not significantly affected by this process. This is in contrast with Ref. [26] using hard particles and faster force dynamics, where time filtering is needed on the photoelastic data to connect to the intruder dynamics.

We first make the general observation that TP curves are highly similar in shape to the photoelastic intensity and acceleration of the intruder, suggesting that the material response responsible for slowing down the intruder involves the formation of a highly structured force field. It is not only that the particles exposed to impact light up, but they respond in a manner that corresponds to a strongly nonuniform force field. The strongest deacceleration of the intruder [the peak in Fig. 3(d)] corresponds (approximately) to the maximum values of TP_0 and TP_1.

We observe particularly good agreement among TP_1, photoelastic intensity, and acceleration. Examining the acceleration curve in Fig. 3(d), we note that there is a primary peak, corresponding to forces building up beneath the intruder and relaxing, but then there is a secondary rise at roughly 0.008 s. This event is clearly visible in movies of the impact; see [47]. TP_1 captures the secondary rise in the acceleration at roughly 0.008 s, while TP_0 does not follow the acceleration and photoelastic intensity accurately. This result already suggests that the properties of the loops, in particular, play an important role in determining the dynamics of the intruder.

Figure 4 shows another example of impact on soft particles. This example is interesting since it shows particularly clearly the correlation between the TP_1 and the acceleration of the intruder. For this experiment, the agreement between TP_1 and acceleration is even better than the agreement between photoelastic intensity and acceleration. We conclude that the

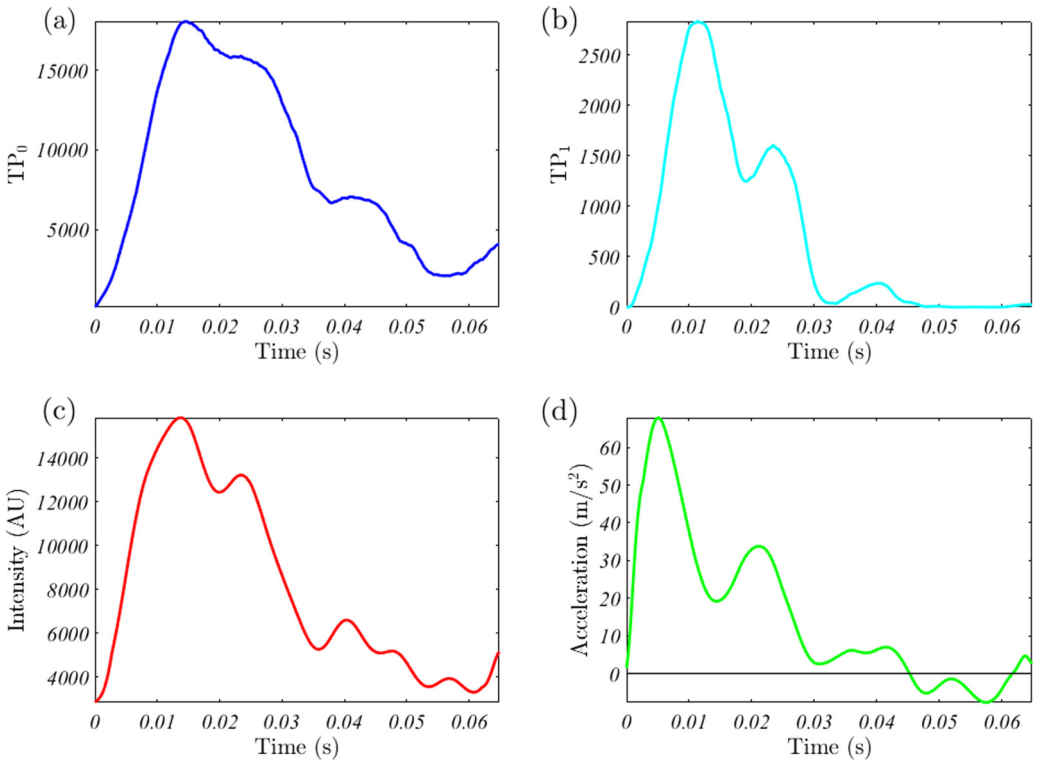

FIG. 4. Total persistence for the components, TP_0, for the loops, TP_1, the photoelastic intensity, and the intruder's acceleration for the impact on soft particles (soft 6.35–1.3).

strong presence of loops in the force networks (as quantified by the TP_1) appears to plays an important role in determining the intruder's dynamics.

Table I shows in precise terms the degree of correlation between the various topological measures, photoelastic intensity, and the acceleration of the intruder for the 10 considered experiments. In addition to $TP_{0,1}$, the table also shows $TC_{0,1}$, defined as the total number of generators for the components and loops, respectively. This measure appears to also show a similar level of correlation as TP. Across the board, we find high correlation for the measures related to loops, showing once again that the loops play an important role across different impact speeds and different particle properties. The correlation of the measures related to loops is comparable to the correlation of the photoelastic intensity.

TABLE I. The correlations between acceleration and various topological measures and photoelastic intensity for different experiments with varying particle stiffness, intruder diameter D, and initial impact velocity v_0. The value of 1 would correspond to perfect correlation, while 0 would mean a complete lack of correlation.

Particle type	D (cm)	v_0 (m/s)	TP_0	TP_1	TC_0	TC_1	Intensity
medium	6.35	2.2	0.86	0.64	0.73	0.82	0.86
medium	6.35	3.2	0.84	0.73	0.75	0.73	0.91
medium	6.35	4.9	0.73	0.78	0.73	0.82	0.91
medium	12.7	2.6	0.35	0.70	−0.53	0.68	0.88
medium	12.7	3.8	0.80	0.81	0.77	0.88	0.90
medium	12.7	4.5	0.85	0.78	0.74	0.83	0.96
medium	20.32	2.3	0.79	0.88	0.76	0.86	0.92
soft	6.35	1.3	0.61	0.88	0.46	0.85	0.80
soft	6.35	2.3	0.50	0.79	0.06	0.66	0.68
soft	6.35	3.4	0.34	0.81	0.05	0.63	0.52
	average		0.67	**0.78**	0.44	**0.77**	**0.83**

For all experiments using soft particles, the correlation values for TP_1 are larger than those for the photoelastic intensity (admittedly, with a small sample size). This is likely related to the fact that the photoelastic intensity of a given particle under compression forces will saturate at a given deformation, and fringes will begin to appear (see Fig. 1 from Ref. [30] and Fig. 7 from Ref. [24]). Extracting force information on a per-particle basis past the saturation force is impossible unless the fringes themselves are analyzed, but this requires images with higher resolution than we can obtain. Since soft particles are more easily deformed than medium stiffness particles, they have a smaller saturation force, and we reach this saturation regime more easily. Thus, for soft particles, the photoelastic intensity begins to break down as a good measure of the intruder dynamics, particularly for higher speed impacts with larger forces where more particles tend to be saturated. Perhaps surprisingly, the network structure appears to preserve some information that is lost when the photoelastic intensity saturates, and we are able to extract it via TP_1.

Since TP provides such a good description of the dynamics of the intruder, one may wonder whether some simpler quantity could provide a similarly good description. For example, one could ask whether it is indeed necessary to employ a relatively complicated concept of persistence in the first place, and whether instead one could resort to a simpler measure, such as Betti numbers, which were shown to be useful in describing

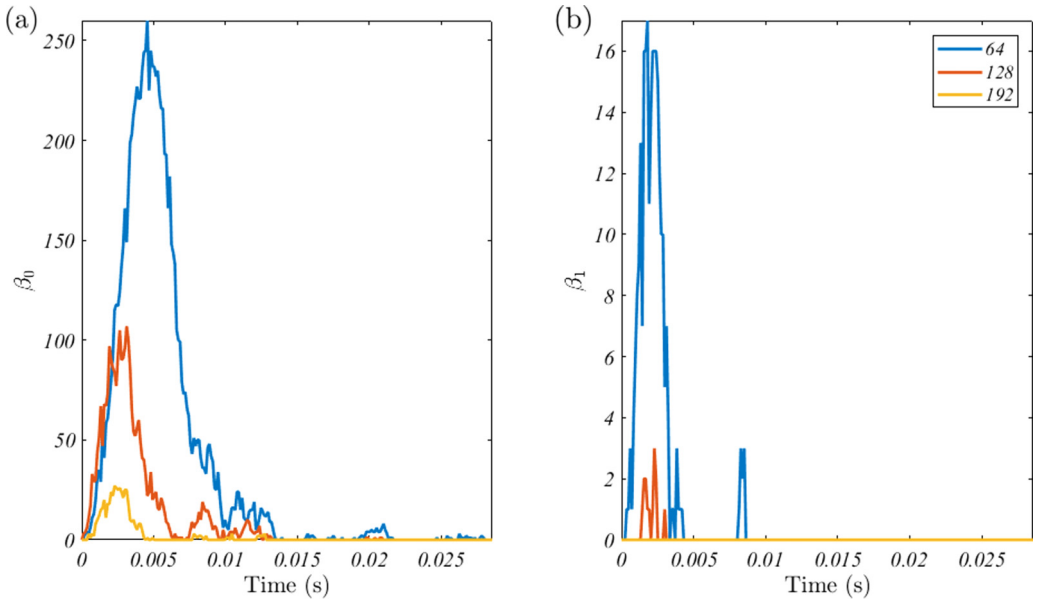

FIG. 5. Betti numbers, β_0 (a) and β_1 (b), for the reference case, respectively. No smoothing is used here since the amount of data, particularly for β_1, is limited. The results are shown for three different brightness threshold levels, as discussed in the text.

force networks in simulated granular systems exposed to compression [40]. In Sec. II C we described how to compute Betti numbers from the persistence, however Betti numbers could be computed directly as well by simply counting the number of components and loops for a given intensity threshold. Figure 5 shows the Betti numbers, β_0 and β_1 for the reference case, and for a few different threshold levels. Clearly, as the threshold level is increased, the number of components and loops decreases sharply, particularly for the loops. Also, by comparison with Fig. 3, we note that the degree of agreement between the acceleration and photoelastic intensity for Betti numbers is much weaker. This is not surprising since Betti numbers provide only partial information. Therefore, one cannot expect such a precise correlation with the intruder's dynamics and photoelastic intensity as was the case with the TP. In addition, by definition Betti numbers involve a choice of threshold, therefore any conclusion obtained using Betti numbers is based on an (arbitrary) choice.

B. Material response: Time evolution of networks

Our analysis thus far has focused on topological properties of stationary networks (that is, one image at a time). However, persistent homology also allows for extraction of information on the evolution of force networks using the distance concept discussed in Sec. II. Calculation of distance is computationally demanding, since the analysis of a single experiment involves comparing a large number of images, and each image includes a large number of generators [the computational cost of carrying the computation is $O(N^3)$, where N is the number of generators]. Of course, one could skip the images to simplify the calculations (we will do this in what follows, although for

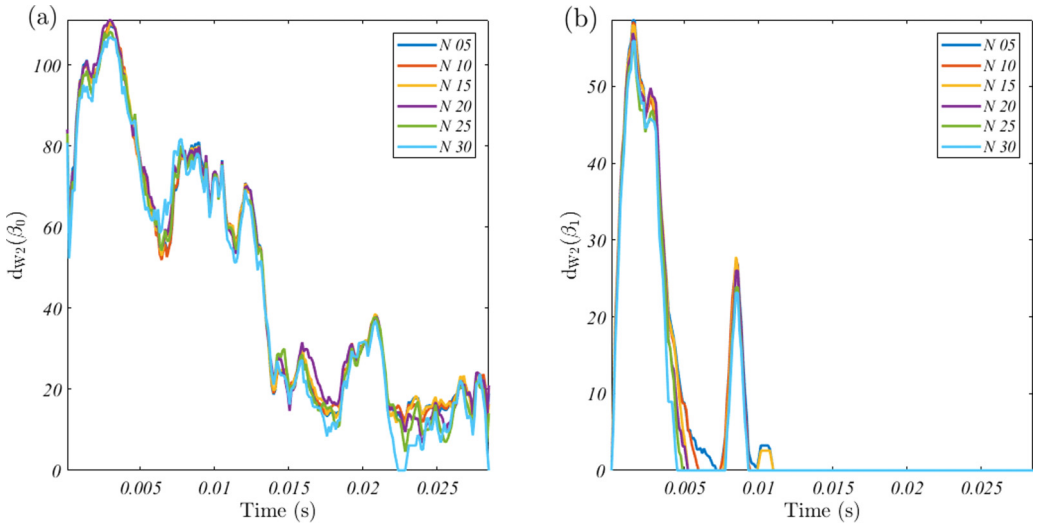

FIG. 6. Wasserstein distance between the consecutive images for the reference case as a different amount of noise (shown by the values of N in the legends) is assumed for components (a) and loops (b). The distances are essentially insensitive to noise.

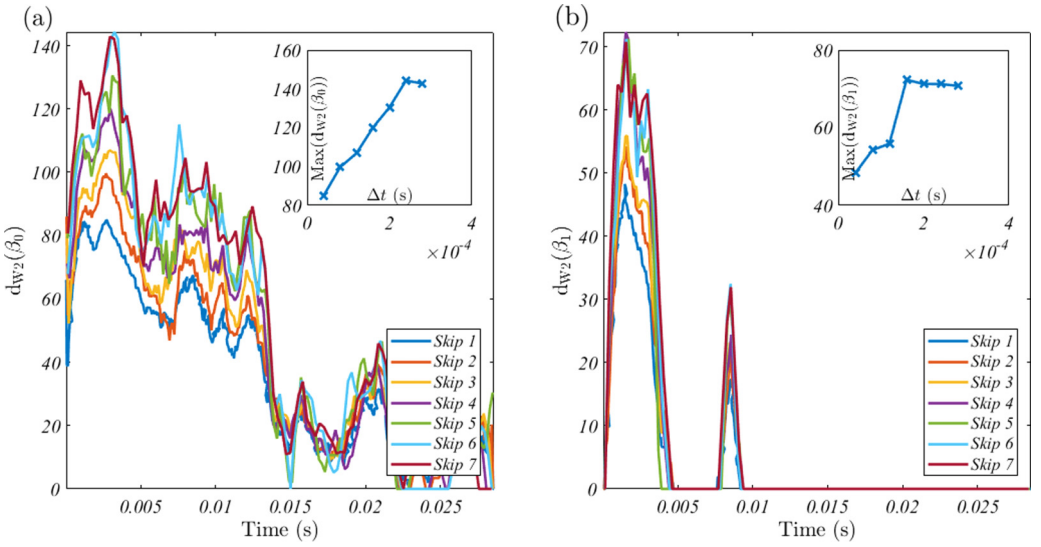

FIG. 7. Wasserstein distance between the images [(a) components; (b) loops] for the reference case assuming that the generators closer than 30 pixels to the diagonal can be ignored. The given number of "skips" specifies the number of images that were skipped in the calculation of the Wasserstein distance. The insets show how the maxima of the distances depend on the time interval between the images considered. For the insets, Δt on the horizontal axes correspond to the number of skipped images multiplied by the time between two consecutive images, which is given by the inverse frame rate. Since the data for the maxima are noisy, we smoothed the distances data from the main panels for the purpose of calculating the maxima shown in the insets.

a different purpose); however, such an approach leads to a loss of information.

Another approach that is more appropriate is based on the fact that the persistence diagrams involve a large number of generators close to the diagonal; see Sec. II C and the Supplemental Material [47]. These generators could be thought of as noise, since they represent the features that persist only for a very small range of the force thresholds or image brightness levels; this range may even be close to the accuracy of the process leading to the analyzed experimental images. Therefore, it makes sense to remove some of the generators very close to the diagonal. Since there are many generators there, the computations that ignore these generators can be carried much faster. Figure 6 shows the results obtained if the generators living during less than or equal to the specified number of brightness levels are not considered: we see that the distance between the images is essentially insensitive if the generators up to 30 levels from the diagonal are removed. We therefore carry out further computations of the distance, ignoring the generators that are closer than 30 levels to the diagonal.

Figure 7 shows the results obtained for the distance if the specified number of images is skipped in calculations. The results show that, as expected, the distance between the images increases with the number of skipped images. However, the increase is slow: even if only every seventh image is considered, the distance increases by less than a factor of 2; see, in particular, the insets in Fig. 7. The significance of this finding is as follows: if the evolution of the force field were completely resolved, the distance should have increased linearly with the number of images skipped (a simple argument for why linear growth should be expected is that the distance function could be approximated by a linear function for two diagrams that are arbitrarily close; see [42,43] for further discussion regarding this issue). This is not the case, however, showing that the evolution of the force field during impact is *not* completely resolved, meaning that the force field evolves on the time scale that is faster than the inverse sampling rate used. While, based on the results provided, we do not know what the time scale is on which the force networks evolve, at least the presented results provide a lower bound. The final conclusion is therefore that the force network evolves on the time scale that is not completely captured by the experimental imaging. We note that the same conclusions can be reached by considering soft particles (figures not shown for brevity).

IV. CONCLUSIONS

In this paper, we have shown the utility of persistent homology in analyzing the results of physical experiments that are difficult to analyze via other means. Due to the fast dynamics and finite resolution of the experimental images, the available data are inherently limited. Even so, persistent homology provides meaningful and insightful results regarding the structure of the force networks in a granular system during impact from an intruder.

Persistent homology allows quantification of structural or geometrical properties of the force networks. This analysis has shown, for a set of 10 considered experiments that involve different impact speeds and different particle properties, that the loop structure of the force networks is crucial in understanding material response and the dynamics of the intruder. We again point out that this conclusion does not involve the concept of a force threshold: it extends over all force thresholds. Therefore, we avoid making an arbitrary choice for a force threshold. Furthermore, we note that the utility of persistent homology is not limited to two spatial dimensions (2D): as long as the data are available, a similar type of analysis can be carried out in 3D.

The tools of persistent homology also allow quantification of dynamical properties of the force networks. We have shown a quantitative comparison between images obtained at different times during the experiments. This comparison allows us further to discuss the time scale on which force networks evolve. Surprisingly, we are able to show that the evolution happens on the time scale that is faster than the inverse frame rate used in the experiments. Further work will be needed to capture this time scale in more precise terms.

ACKNOWLEDGMENTS

The experiments discussed in the present paper were carried out in the laboratory of Robert P. Behringer at Duke University. The authors also acknowledge many useful discussions with Lenka Kovalcinova, as well as with the members of the computational topology group at Rutgers University, especially Rachel Levanger, Miroslav Kramár, and Konstantin Mischaikow. This work was supported in part by the NSF Grant No. DMS-1521717 and DARPA Grant No. HR0011-16-2-0033.

[1] H. J. Moore, J. M. Boyce, and D. A. Hahn, Small impact craters in the lunar regolith—Their morphologies, relative ages, and rates of formation, Moon Planets **23**, 231 (1980).

[2] J. E. Colwell and M. Taylor, Low-velocity microgravity impact experiments into simulated regolith, Icarus **138**, 241 (1999).

[3] M. Raibert, K. Blankespoor, G. Nelson, and R. Playter, Bigdog, the rough-terrain quadruped robot, IFAC Proc. Vol. **41**, 10822 (2008).

[4] C. Li, T. Zhang, and D. I. Goldman, A terradynamics of legged locomotion on granular media, Science **339**, 1408 (2013).

[5] D. Stöffler, D. E. Gault, J. Wedekind, and G. Polkowski, Experimental hypervelocity impact into quartz sand: Distribution and shock metamorphism of ejecta, J. Geophys. Res. **80**, 4062 (1975).

[6] J.V. Poncelet, *Course de Me'canique Industrielle* (Lithographie de Clouet, Paris, 1829).

[7] W. A. Allen, E. B. Mayfield, and H. L. Morrison, Dynamics of a projectile penetrating sand, J. Appl. Phys. **28**, 370 (1957).

[8] M. J. Forrestal and V. K. Luk, Penetration into soil targets, Int. J. Impact Eng. **12**, 427 (1992).

[9] K. A. Newhall and D. J. Durian, Projectile-shape dependence of impact craters in loose granular media, Phys. Rev. E **68**, 060301 (2003).

[10] J. S. Uehara, M. A. Ambroso, R. P. Ojha, and D. J. Durian, Low-Speed Impact Craters in Loose Granular Media, Phys. Rev. Lett. **90**, 194301 (2003).

[11] M. P. Ciamarra, A. H. Lara, A. T. Lee, D. I. Goldman, I. Vishik, and H. L. Swinney, Dynamics of Drag and Force Distributions for Projectile Impact in a Granular Medium, Phys. Rev. Lett. **92**, 194301 (2004).

[12] M. A. Ambroso, C. R. Santore, A. R. Abate, and D. J. Durian, Penetration depth for shallow impact cratering, Phys. Rev. E **71**, 051305 (2005).

[13] H. Katsuragi and D. J. Durian, Unified force law for granular impact cratering, Nat. Phys. **3**, 420 (2007).

[14] D. I. Goldman and P. Umbanhowar, Scaling and dynamics of sphere and disk impact into granular media, Phys. Rev. E **77**, 021308 (2008).

[15] E. L. Nelson, H. Katsuragi, P. Mayor, and D. J. Durian, Projectile Interactions in Granular Impact Cratering, Phys. Rev. Lett. **101**, 068001 (2008).

[16] P. Umbanhowar and D. I. Goldman, Granular impact and the critical packing state, Phys. Rev. E **82**, 010301 (2010).

[17] T. A. Brzinski III, P. Mayor, and D. J. Durian, Depth-Dependent Resistance of Granular Media to Vertical Penetration, Phys. Rev. Lett. **111**, 168002 (2013).

[18] K. N. Nordstrom, E. Lim, M. Harrington, and W. Losert, Granular Dynamics During Impact, Phys. Rev. Lett. **112**, 228002 (2014).

[19] Z. Chen, M. Omidvar, M. Iskander, and S. Bless, Modelling of projectile penetration using transparent soils, Int. J. Phys. Model. Geo. **14**, 68 (2014).

[20] J. J. S. Jerome, N. Vandenberghe, and Y. Forterre, Unifying Impacts in Granular Matter from Quicksand to Cornstarch, Phys. Rev. Lett. **117**, 098003 (2016).

[21] T. Wakabayashi, Photoelastic method for determination of stress in powder mass, in *Proceedings of the 9th Japan National Congress for Applied Mechanics* (Science Council of Japan, Tokyo, 1960), pp. 133–140.

[22] T. Takada, M. Kuramoto, T. Kunio, and H. Kuno, A feasibility study of scattered-light photoelasticity in the determination of the side pressure distribution of the pressed powder bed, Powder Technol. **14**, 51 (1976).

[23] G. W. Baxter, Stress distributions in a two dimensional granular material, in *Powders & Grains 97*, edited by R. P. Behringer and J. T. Jenkins (Balkema, Rotterdam, 1997), pp. 345–348.

[24] K. E. Daniels, J. E. Kollmer, and J. G. Puckett, Photoelastic force measurements in granular materials, Rev. Sci. Instrum. **88**, 051808 (2017).

[25] A. H. Clark, A. J. Petersen, L. Kondic, and R. P. Behringer, Nonlinear Force Propagation During Granular Impact, Phys. Rev. Lett. **114**, 144502 (2015).

[26] A. H. Clark, L. Kondic, and R. P. Behringer, Particle Scale Dynamics in Granular Impact, Phys. Rev. Lett. **109**, 238302 (2012).

[27] A. H. Clark, A. J. Petersen, and R. P. Behringer, Collisional model for granular impact dynamics, Phys. Rev. E **89**, 012201 (2014).

[28] A. H. Clark and R. P. Behringer, Granular impact model as an energy-depth relation, Europhys. Lett. **101**, 64001 (2013).

[29] A. H. Clark, L. Kondic, and R. P. Behringer, Steady flow dynamics during granular impact, Phys. Rev. E **93**, 050901 (2016).

[30] T. S. Majmudar and R. P. Behringer, Contact force measurements and stress-induced anisotropy in granular materials, Nature (London) **435**, 1079 (2005).

[31] T. S. Majmudar, M. Sperl, S. Luding, and R. P. Behringer, The Jamming Transition in Granular Systems, Phys. Rev. Lett. **98**, 058001 (2007).

[32] J. F. Peters, M. Muthuswamy, J. Wibowo, and A. Tordesillas, Characterization of force chains in granular material, Phys. Rev. E **72**, 041307 (2005).

[33] A. Tordesillas, D. M. Walker, and Q. Lin, Force cycles and force chains, Phys. Rev. E **81**, 011302 (2010).

[34] A. Tordesillas, D. M. Walker, G. Froyland, J. Zhang, and R. P. Behringer, Transition dynamics of frictional granular clusters, Phys. Rev. E **86**, 011306 (2012).

[35] D. S. Bassett, E. T. Owens, K. E. Daniels, and M. A. Porter, Influence of network topology on sound propagation in granular materials, Phys. Rev. E **86**, 041306 (2012).

[36] M. Herrera, S. McCarthy, S. Slotterback, E. Cephas, W. Losert, and M. Girvan, Path to fracture in granular flows: Dynamics of contact networks, Phys. Rev. E **83**, 061303 (2011).

[37] D. M. Walker and A. Tordesillas, Taxonomy of granular rheology from grain property networks, Phys. Rev. E **85**, 011304 (2012).

[38] R. Arévalo, I. Zuriguel, and D. Maza, Topology of the force network in jamming transition of an isotropically compressed granular packing, Phys. Rev. E **81**, 041302 (2010).

[39] R. Arévalo, L. A. Pugnaloni, I. Zuriguel, and D. Maza, Contact network topology in tapped granular media, Phys. Rev. E **87**, 022203 (2013).

[40] L. Kondic, A. Goullet, C. S. O'Hern, M. Kramár, K. Mischaikow, and R. P. Behringer, Topology of force networks in compressed granular media, Europhys. Lett. **97**, 54001 (2012).

[41] M. Kramár, A. Goullet, L. Kondic, and K. Mischaikow, Persistence of force networks in compressed granular media, Phys. Rev. E **87**, 042207 (2013).

[42] M. Kramár, A. Goullet, L. Kondic, and K. Mischaikow, Quantifying force networks in particulate systems, Physica D **283**, 37 (2014).

[43] M. Kramár, A. Goullet, L. Kondic, and K. Mischaikow, Evolution of force networks in dense particulate media, Phys. Rev. E **90**, 052203 (2014).

[44] L. A. Pugnaloni, C. M. Carlevaro, M. Kramár, K. Mischaikow, and L. Kondic, Structure of force networks in tapped particulate systems of disks and pentagons I: Clusters and loops, Phys. Rev. E **93**, 062902 (2016).

[45] L. Kondic, M. Kramár, L. A. Pugnaloni, C. M. Carlevaro, and K. Mischaikow, Structure of force networks in tapped particulate systems of disks and pentagons II: Persistence analysis, Phys. Rev. E **93**, 062903 (2016).

[46] Available at http://chomp.rutgers.edu.

[47] See Supplemental Material at http://link.aps.org/supplemental/10.1103/PhysRevE.97.012906 for an animation of persistence diagrams for the reference case (persistence-diagrams.mp4.), and an animation of total persistence, photoelastic intensity, and acceleration (persistence-lifespan.mp4).